Hindawi
International Journal of Aerospace Engineering
Volume 2018, Article ID 6378635, 15 pages
https://doi.org/10.1155/2018/6378635

Research Article

Sensor-Driven Preliminary Wing Ground Plane Sizing Approach and Applications

Ankur S. Patil and Emily J. Arnold

University of Kansas, Lawrence, KS 66045, USA

Correspondence should be addressed to Emily J. Arnold; earnold@ku.edu

Received 25 July 2017; Accepted 18 April 2018; Published 2 July 2018

Academic Editor: Angel Velazquez

Structurally integrated antenna arrays provide synergies allowing the integration of large apertures onto airborne platforms. However, the surrounding airframe can greatly impact the performance of the antenna array. This paper presents a sensor-driven preliminary wing ground plane sizing approach to provide insight into the implications of design decisions on payload performance. The improvement of a wing-integrated antenna array that utilizes the wing as a ground plane motivated this study. Relationships for wing span, wing chord, and thickness are derived from extensive parametric electromagnetic simulations based on optimum antenna performance. It is expected that these equations would be used after an initial wing-loading design point has been selected to provide the designer guidance into how various wing parameters might affect the integrated antenna performance.

1. Introduction

Airborne remote sensing using active radars has become an effective tool in geoscience fields for conducting Earth observations [1–3]. Compared to satellite observations, airborne platforms are capable of spatially finer-resolution measurements over large areas. Unmanned Aircraft System (UAS) platforms and sensors are of particular interest for remote sensing of polar regions as well as other harsh regions. Increasing civilian access to UAS for remote sensing applications requires advances in electronic hardware, sensors, and platforms. One technological advancement that will help realize the next generation of airborne remote sensing platforms and sensors is the development of Multifunctional Aircraft Structures (MAS). Multifunctional structures are primary and secondary aircraft structures that have been designed to operate as antennas. For airborne remote sensing applications with UAS, this type of structure offers potential configuration synergies that could result in reduced payload weight, increased sensor performance, and increased aircraft performance, particularly for airframe-integrated phased antenna arrays.

The research field of MAS combines the disciplines of aerospace structures and electromagnetics. The primary technical challenge associated with the design of MAS is that the design requirements of the two dissimilar fields often conflict. Aircraft flight regimes often limit the size of antenna apertures, and creating structures that are aerodynamically and structurally efficient while also satisfying electrical requirements is often difficult. In addition, structural deformations, airframe material, and vibrations have all been shown to affect antenna performance [4–9].

While MAS are the ideal approach for integrating payload antennas, this approach requires either significant changes to existing airframes or consideration of MAS during the original design of the vehicle. As is most often the case when major airframe modification is not an option or operating frequencies are too low, large antenna structures cannot be integrated into the vehicle mold line; instead, they require externally mounted support structures. However, even externally mounted antennas are similarly affected by the surrounding airframe and support structure.

Two examples of wing-integrated antenna arrays are shown in Figure 1. The Meridian UAS (Figure 1(a)) was

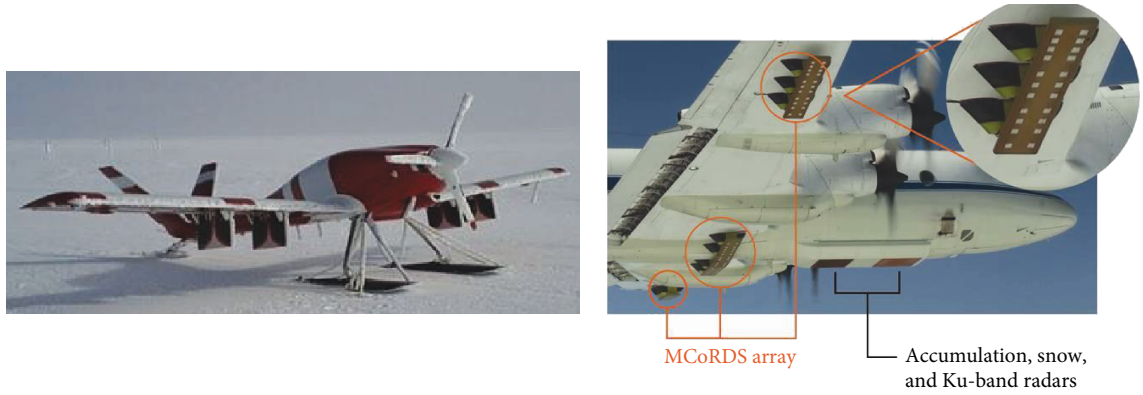

(a) (b)

Figure 1: Meridian UAS with four Vivaldi antennas integrated below wing [16] (a) and NASA P-3 with all sensors installed [9] (b).

designed to house an ice-sounding radar and a large cross-track antenna array for sounding ice thickness and bedrock topography in the cryosphere. This UAS was designed and manufactured by faculty and students at the University of Kansas Aerospace Engineering department [10–13]. The Meridian is a low-wing, propeller-driven medium-range vehicle with a range of about 1760 km and cruise speed of 68.4 m/s. The wing-mounted antenna array consists of eight Vivaldi antenna elements originally designed for the Meridian ice depth sounder radar system, which operates from 180 to 210 MHz [14–15]. The Meridian wings, which serve as the antenna-ground plane, are made of carbon fiber composite material, which is both electrically lossy and conductive.

The NASA P-3B (Figure 1(b)) has flown a four-radar instrument suite, including the ice depth sounder as part of the NASA Operation IceBridge Campaign [9]. As shown in Figure 1, the depth sounder antenna array is mounted under the wings and fuselage via 10 hardpoints. The other three radar systems are integrated into the bomb bay. The wing-mounted antenna array consists of 15 modified planar dipole antennas—four on each wing and seven under the fuselage belly. Similar to the Meridian system, the wing of the P-3 acts as a ground plane for the dipole antennas to improve the array gain and directivity. The antennas are located a quarter wavelength below the airframe (~0.38 m).

The ground plane plays a vital role in improving the electrical performance of an antenna as it improves the antenna element gain [17–18] and directivity (~7–9 dB) [18], increases the front-to-back ratio (FTBR) [18], reduces the electrical size of an antenna [19], and can be used to tune the antenna resonant frequency [19]. Investigations into the effects of ground plane size on antenna performance have primarily focused on microstrip patch antenna designs. The near proximity of the ground plane edges to the radiating element as well as the overall size of a patch antenna's ground plane greatly impacts its radiation characteristics. As the demand and application of patch antennas grew in the mid-1980s through early 1990s, precise mathematical methods were needed to better predict the antenna response, particularly in the presence of a finite ground plane. Huang [20] and Lier and Jakobsen [21] used diffraction theory to calculate the diffracted field created by the edge of a finite ground plane, while several other groups used the method of moments to calculate induced currents on the ground plane whose resulting field components contribute to the overall radiation characteristics of the antenna [17, 22].

With the recent proliferation of physics-based simulation software, the impact of the finite ground plane on the overall radiation characteristics is accounted for in the full-wave solution of a 3D model. Studies on the effects of finite ground planes have now shifted from simply trying to accurately capture these effects for microstrip patch antennas to now optimizing the design with as small of a ground plane as possible [23–24]. Microstrip patch antennas are used when low-profile, lightweight antenna designs are required, and the goal of many of these ground plane studies is to minimize the size of the antenna (hence ground plane) while maintaining acceptable antenna performance. In addition, Cung et al. [25] and Huff and Bernhard [26] have both investigated the application of serrated ground plane edges to mitigate the effects of ground plane edges in close proximity to the radiating element. A ground plane edge treatment such as serrations helps in reducing edge diffraction and reflections while improving the element's radiation characteristics [25]. In addition, ground plane edge serrations have also been shown to improve polarization characteristics and radiation bandwidth [26].

The effects of ground plane size have not been studied as extensively for other antenna types or for lower frequencies as it has been for patch antennas. This is largely due to the stricter size limitations when considering microstrip patch antenna applications. As mentioned earlier, patch antennas are preferred for applications that require low-profile designs. Though the ground plane size for a patch antenna is comparatively smaller than the one typically used or a dipole antenna due to operating frequency and space limitations, both antenna designs exploit the advantages of a ground plane in the same manner. For our application of wing-integrated dipole antenna arrays that utilize the wing as the ground plane, ground plane size limitations are a much bigger factor than they are for ground-based, or even space-based applications. Another unique aspect

of our application is that the size and shape of the ground plane are not driven by the sensor performance, but rather by the vehicle performance.

In this paper, we present a series of parametric studies in support of developing a preliminary wing and ground plane-sizing approach based on antenna performance. The purpose of this study is to provide insight for future aircraft design, particularly UAS with wing-integrated sensors. This study aims to provide a foundation to integrate sensor-based design considerations into typical aircraft design processes, such as those in [27, 28]. This type of sensor-driven design approach could be an incredibly valuable tool for future vehicle design—particularly for UAS, as the purpose of these vehicles is to carry sensors and there is little reason to fly the vehicle if the payload does not meet performance requirements.

Section 2 presents simulation results for a single antenna by systematically changing three variables of the wing ground plane, namely, length (span), width (chord), and vertical offset (thickness-to-chord ratio). These results are used as the foundation to develop wing sizing relationships for optimal antenna performance. In Section 3, the wing sizing study is extended to multielement antenna arrays to demonstrate the robustness of the relationships developed in Section 2 for a single antenna element. Finally, Section 4 presents the conclusions drawn from the study, and a discussion of its limitations and how the relationships described here could be utilized for future aircraft design.

2. Sensor-Driven Preliminary Wing Sizing

2.1. Overview of Study Parameters. In the following sections, we present simulated antenna results which will be used to develop the foundation of this sizing approach. Assuming a metallic portion of the wing would be used as a ground plane for the wing-integrated antenna array, we examine how the antenna gain in the nadir direction and resonant frequency are affected by wing attributes such as span, chord, and thickness-to-chord ratio. Gain in the nadir direction was specifically examined since the wing ground plane is utilized to direct the energy in the nadir direction. Since it is tedious to capture the performance of all types of antennas, the study is based on the performance of the half-wavelength dipole antenna, due to its lower profile attributes and commonality. Figure 2 shows a schematic of the planar dipole. At the outset of the study, the antennas were tuned to the appropriate frequency. The widths of the dipoles were maintained at a constant 10% of the resonant wavelength (λ) for all frequencies, and due to the finite width, the antennas typically resonated at a total length of 0.41λ rather than 0.5λ.

The wing ground plane sizing studies are repeated at four different resonating frequencies—100 MHz, 200 MHz, 1 GHz, and 2 GHz. The purpose for repeating the study at these frequencies is to verify that the trends observed are independent of frequency. In addition, the wing dimensions are expressed as a percentage of wavelength such that the results are independent of operating frequency

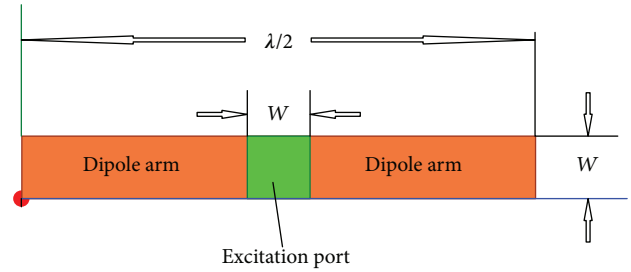

Figure 2: Schematic of dipole dimensions.

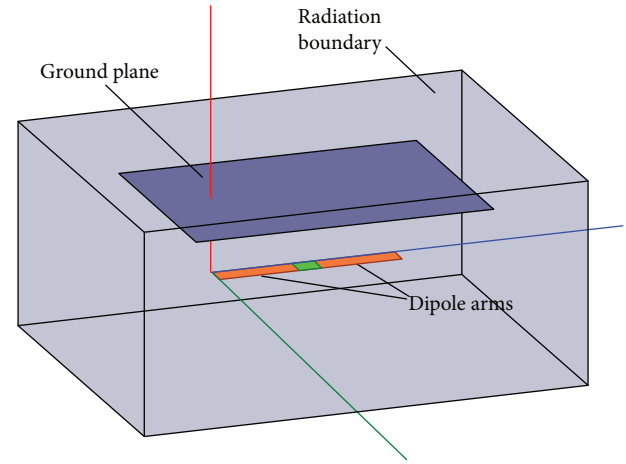

Figure 3: A simulation setup for the dipole antenna with a ground plane.

and more broadly applicable to any dipole antenna. Parametric simulations were completed using ANSYS HFSS [29] software, and over 400 simulations were performed to determine the relationships between the wing dimensions and antenna performance.

Figure 3 shows the simulation setup for an antenna with ground plane which includes antenna element(s), a ground plane, an air box that defines the solution space, and a 50-ohm port between dipole arms that feeds the antenna. Perfect electrical conductor (PEC) properties were given to all conductive components, including the antenna arms and the ground plane. The air box defining the solution space was given the properties of a vacuum, and the faces of the box were given radiating boundary conditions. The walls of the box were kept at least a quarter of a wavelength from any component. The frequency ranges (sweep) of the simulations were set according to antenna operating frequency, and a 30–50% bandwidth was used with a frequency step size of 1–0.5% of the resonant frequency. Though the metallic ground plane represents a wing, it should be noted that no additional conductive parts (such as cables or substructure) were included in these simulations. While these details will influence the antenna performance, their effect on antenna performance is left for future study.

2.2. Wing Span Study. To determine the effects of wing span on antenna performance, a single antenna was simulated with a ground plane meant to represent a metallic wing skin

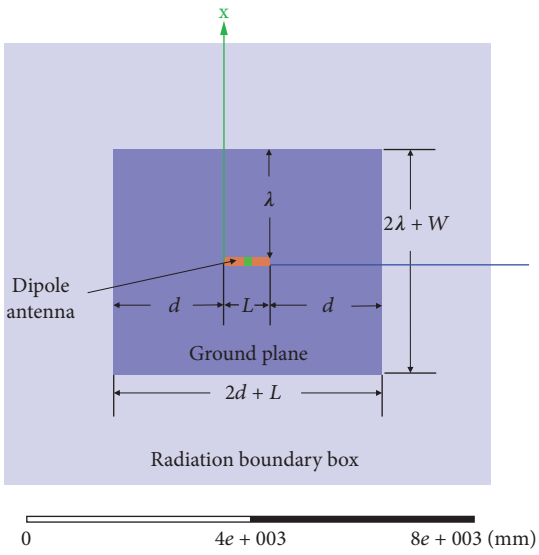

Figure 4: Geometric definitions for the wing span study.

offset from the antenna. This configuration could represent either the upper wing skin acting as the ground plane for an antenna embedded in the lower wing skin or the lower wing skin acting as a ground plane for an antenna offset externally from the wing (as in the case for the NASA P-3 and Meridian UAS shown in Section 1). Then, a parametric analysis was performed by varying the spanwise length. The geometry used to define the parametric simulations is presented in Figure 4. The spanwise length of the ground plane was initially set to $L + 0.1\lambda$, then the distance from the edge of the antenna to the edge of the ground plane, d, was stepped from 5 to 100% of the resonant wavelength, λ, by the step size of 0.05λ. The chordwise width of the ground plane was kept constant and has a total width of $W + 2\lambda$, where W is the width of an antenna and is 10% of wavelength. An offset distance of $\lambda/4$ was maintained between the ground plane and the antenna, as shown in Figure 5. The offset value was determined from well-known image theory that the forward-radiated field and reflected field will constructively add at $\lambda/4$ ground plane spacing [30].

The results from the parametric simulations for the four selected operating frequencies are shown in Figure 6, where frequency shifts and realized gain at nadir are plotted against the ground plane length extension parameter, d, on the two y-axis plot. The frequency shift, f_0, is defined in (1), where f_d is resonant frequency for a corresponding d and f is the original specified operating frequency.

$$f_0 = \frac{(f_d - f)}{f} * 100. \quad (1)$$

It can be seen from the plots that when d is greater than 15% of the corresponding wavelength, the antenna typically resonates within ±0.5% of the specified operating frequency, though in no instances was the frequency shift greater than 1.5%. It is noted that the discrete appearance of the frequency response plot is due to the finite step size used in the simulation. Maximum gain was typically achieved when d was ~0.4λ. In addition, for the gain to be within 0.5 dB of the maximum gain, the ground plane length extension should be between 0.15–0.55λ.

Because the gain in Figure 6 decreases after 0.4λ, the simulation was extended to 5λ to determine the extended trend in the gain. Figure 7 shows the extended simulation results for 100 MHz. As shown in the plot, a local maximum gain is achieved when the length extension parameter is at 40%, 160%, 275%, and 400% of the wavelength. It is also noticed that the magnitude of the local maximum gain decreases as d increases. It can be seen that when d is about 40% of the wavelength, maximum gain without any frequency shift is achieved. The oscillatory trend in the gain due to varying the ground plane size agrees well with what has been published in the literature, not only for patch antennas [17, 22-23] but also for other applications of finite ground planes as well [18, 30].

Based on the findings from the ground plane sizing study, the antenna performance was related to the vehicle's wing sizing. The developed relationship defines the ground plane wing span required to accommodate the antenna array with maximum gain. While determining the wing span required for an antenna array operating at these frequencies, it was found that when d is ~0.4λ, maximum gain is achieved. Though Figure 7 shows that other values of d can produce local maximum gain since these values are much larger than 0.4λ, it would be suggested to add more antenna elements to increase total array gain rather than extend the ground plane unnecessarily. Therefore, the ground plane span relationship was determined using the minimum ideal value of d. From antenna array theory, ideal element center-to-center spacing is $\lambda/2$ [30]. Using the ideal ground plane extension length of 0.4λ found from the plots in Figure 6 and an antenna length of 0.5λ, a relationship for determining the ideal wing span can be derived. Assuming a fuselage diameter, F, the wing ground plane span b suggested for an n-element array is given by

$$b = F + (n + 1.6)\lambda. \quad (2)$$

Figure 8 shows the geometry associated with (2) for a three-element array. Given the operating frequency, number of elements in the array, and an approximate fuselage width, an ideal span can be determined from (2). It should be noted that only the rectangular region outside of the fuselage in Figure 8 is considered the wing ground plane and is metalized. Portions inside the fuselage, leading edge, trailing edge devices, and wing tips are not considered. In the preliminary sizing of the wing, this equation could be used after a wing-loading and power-loading design point (as described in [27]) has been determined. It is noted that the gain sensitivity to the ground plane length is less than 1.5 dB, which is a relatively small change in the antenna performance and is likely due to the orientation of the pattern nulls directed along this axis. As will be shown in the following sections, antenna performance is much more sensitive to other wing geometric parameters.

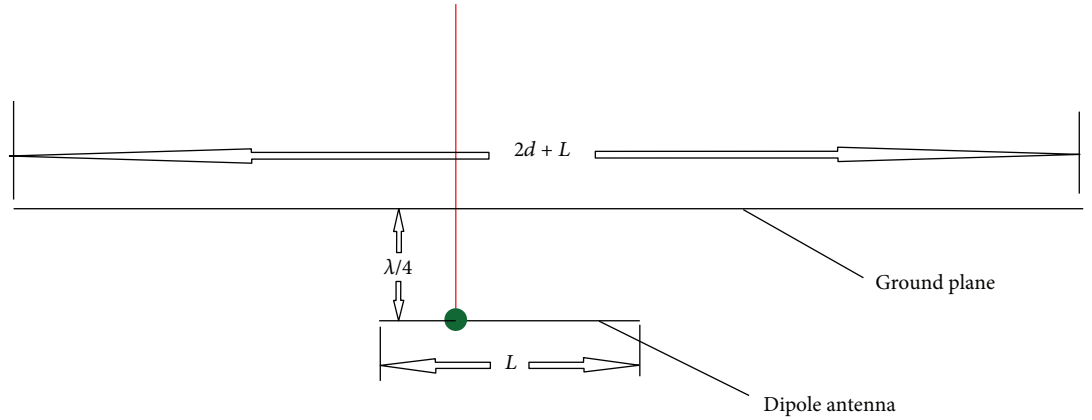

Figure 5: Ground plane offset defined for the wing span study.

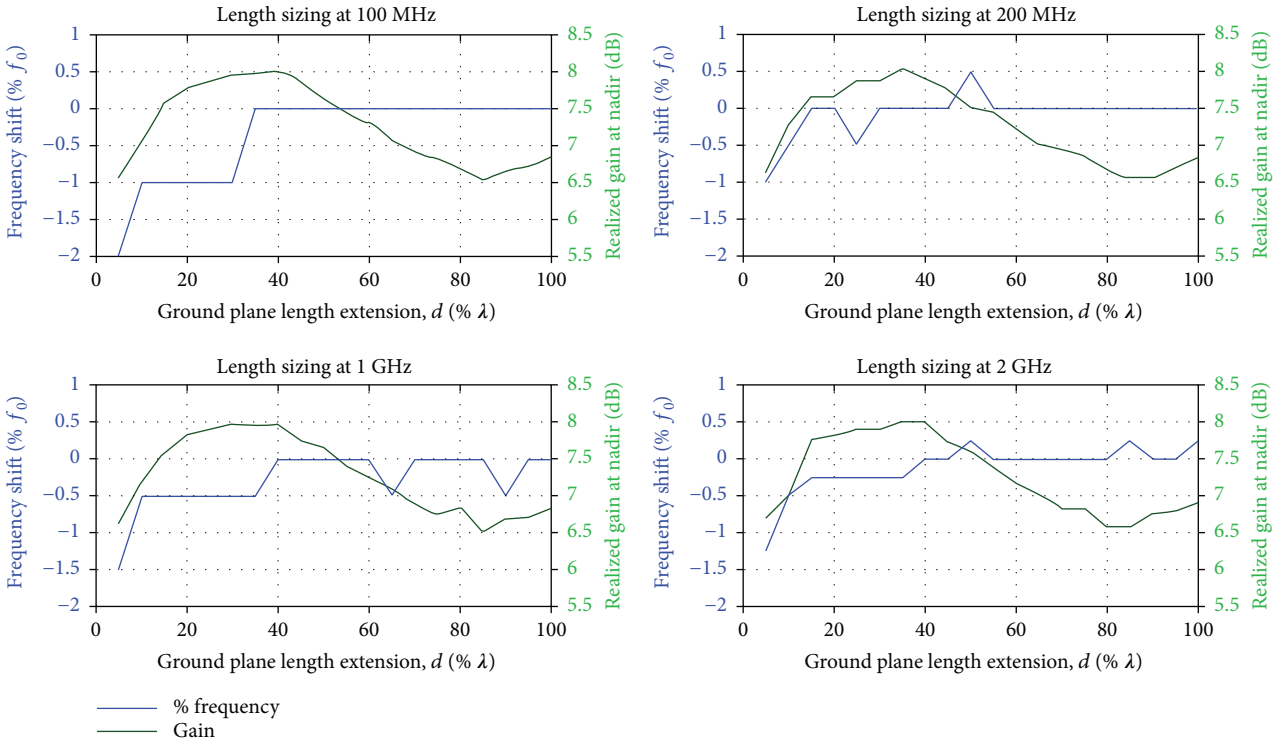

Figure 6: Ground plane length extension versus frequency shift and realized gain at nadir plot for all operating frequencies.

2.3. Wing Chord Study. To determine the effects of the width of the ground plane, the antenna-ground plane offset ($\lambda/4$) as well as the length of the ground plane ($L + 2\lambda$) were kept constant. Initially, the width of the ground plane was set equal to the antenna width plus 0.05λ on either side of the antenna ($W + 0.1\lambda$). The ground plane width extension, d, was then varied by up to one wavelength in 0.05λ increments. Figures 9 and 10 show the geometry associated with the chord sizing study. The frequency shift and realized gain at nadir of the antennas are plotted against d in Figure 11. From the simulation results, it can be concluded that when the ground plane width extension is greater than 20% of the wavelength, the antenna resonates within 0.5% of the desired operating frequency. It can also be seen that when d is about 50% of the wavelength, the maximum gain is achieved without any frequency shift. In addition, as long as the ground plane width extension is at least 25% of a wavelength, the reduction in gain from the maximum value is less than 1 dB. In Figure 11, it is noted that the gain sensitivity to the ground plane width is about 3 dB, almost a 30% increase in gain sensitivity compared to the ground plane length.

As was observed for the ground plane length parameter and as expected, the gain at nadir also had an oscillatory response as a function of the width. The width parameter was simulated out to 5λ, and the gain values were found to vary within 0.5 dB. An explanation for this oscillatory behavior can be found by investigating the current distribution on the ground plane. Similar to the dipole, the current distribution on the ground plane has a sinusoidal pattern along the radial direction. Due to the cyclical spatial variation of the

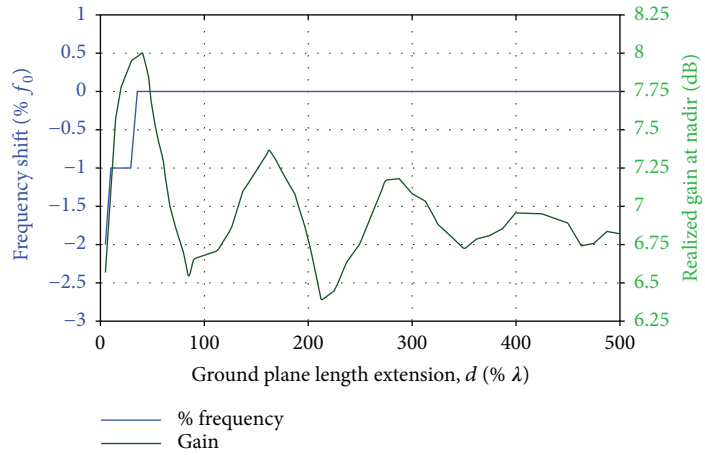

Figure 7: Frequency shift and realized gain for ground plane length extension up to 5λ at 100 MHz.

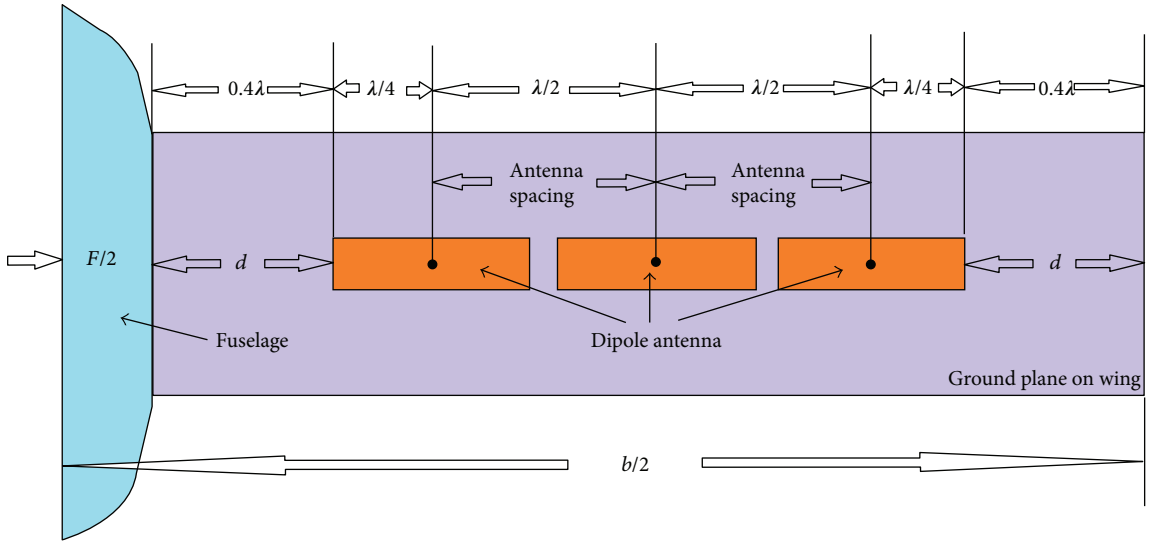

Figure 8: Geometric definition for wing (ground plane) length calculation.

current, every half cycle the current undergoes an 180° phase shift. While the fields generated from the in-phase component will add constructively with the forward-radiated and reflected fields from the antenna, the out-of-phase component will add destructively—thus resulting in the gain reduction. The magnitudes of both the in-phase and out-of-phase currents decrease as the radial distance from the antenna increases, which explains the reduction in gain variation seen in Figure 7.

To determine the relationship for the ideal chord of a wing ground plane, c, based on the antenna performance data in Figure 11, the ground plane width extension is assumed to be $d = 0.5\lambda$. In addition, the portion of the wing chord occupied by control surfaces, high lift devices, and the leading edge is not considered part of the effective ground plane. This is because the variable angle of the control surface/high lift devices and the leading edge will affect the pattern of the antenna; thus, it is beneficial to not consider these portions of the wing as part of the static ground plane. The control surface chord is typically assumed to be 30% of the wing

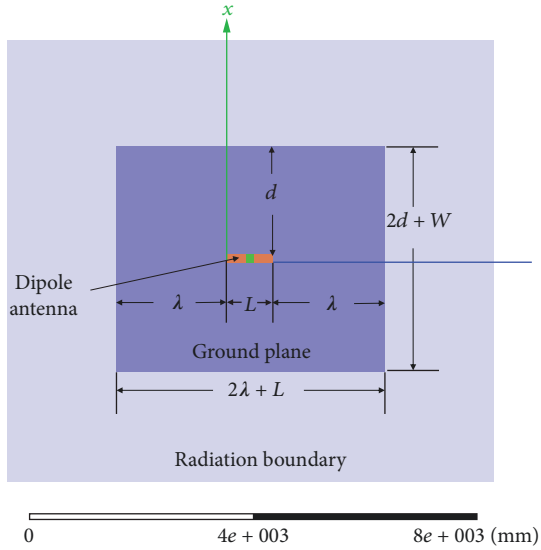

Figure 9: Simulation setup for the wing chord study.

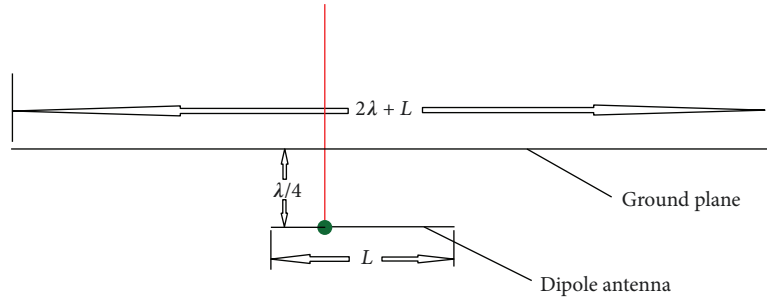

Figure 10: Ground plane offset defined for the wing chord study.

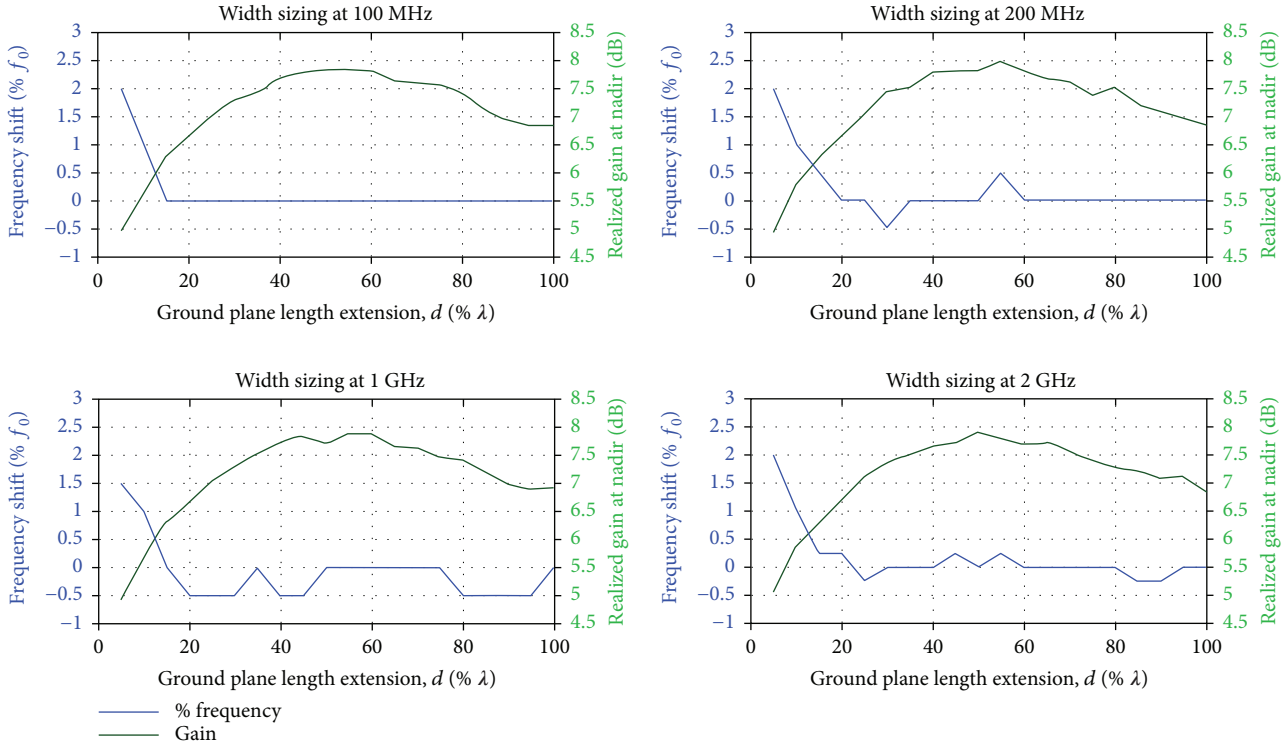

Figure 11: Ground plane width extension versus frequency shift and realized gain at nadir plot for all operating frequencies.

chord [27], and the leading edge surface is assumed to be 20% of the wing chord, as shown in Figure 12. Thus, only 50% of the chord is considered for the wing ground plane. Since the resulting frequency shift is negligible, the chord relationship is derived based on the gain results. Equation (3) shows the relationship in determining the ideal ground plane chord length, c, required for optimum antenna performance in terms of antenna wavelength, λ, and antenna width, W.

$$0.5c = c_{GP} = 2 * \frac{\lambda}{2} + W. \tag{3}$$

Hence, the chord length for the wing, c, becomes

$$c = 2(\lambda + W). \tag{4}$$

Figure 12 shows the geometry associated with (3) and (4), assuming a three-element array. As shown by the gain trends in Figure 11, the antenna gain is expected to be within 1 dB of the maximum value for a ground plane width extension of $d = 0.25\lambda$ or greater. Therefore, a relationship for a minimum recommended wing chord based on a 1 dB reduction in antenna performance becomes

$$c_{\min} = (\lambda + 2W). \tag{5}$$

Similar to (2), it is expected that (4) and (5) would be used to determine a chord after the wing-loading and power-loading design point has been selected. In addition, the span sizing equation and chord sizing equations can be used in combination to determine the ideal ranges of the wing aspect ratio. A comparison between the plots in Figures 6 and 11 suggests that the antenna gain is more sensitive to the ground plane width rather than the length (3 dB variation versus 1.5 dB variation), which again is likely due to the orientation of the dipole antennas and hence the radiation pattern nulls. This sensitivity should be taken under advisement when considering wing aspect ratio.

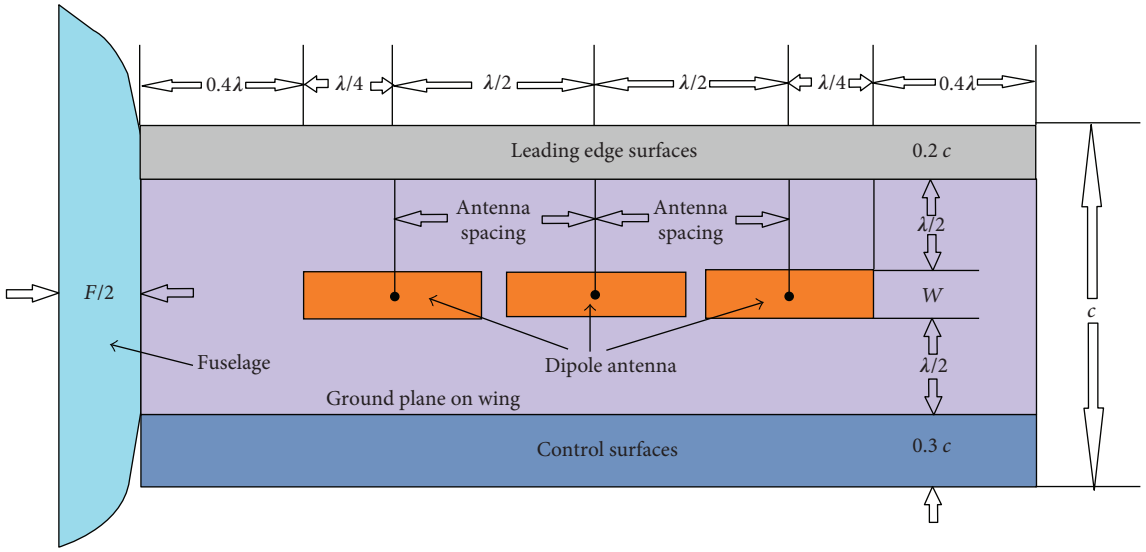

Figure 12: Wing chord geometry associated with (3) and (4).

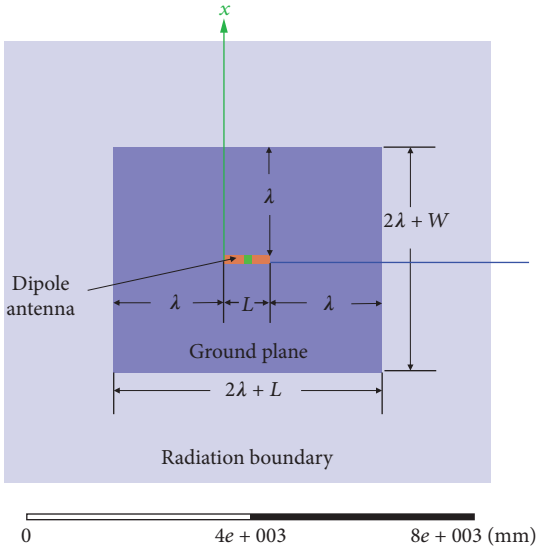

Figure 13: Simulation setup defined for the wing height study.

2.4. Wing Height Study. To determine the antenna sensitivity to the ground plane offset, the antennas were located below a ground plane and the offset was varied. For the dipole antenna, the offset distance, h, between the antenna and the ground plane was varied from 5% to 50% of a wavelength. A ground plane size of $(2\lambda + L) \times (2\lambda + W)$ was used so as to eliminate the ground plane edge effects and to isolate the effect of the offset. The geometry used for the ground plane offset study is shown in Figures 13 and 14. The frequency shift f_0, given by (1), is plotted against ground plane offset distance, h, in Figure 15. This plot shows that the antenna resonance is affected significantly more by the ground plane offset than either the span or chord width. The gain of the antennas at nadir is plotted against ground plane offset in Figure 16, as well as the azimuth angle of maximum gain. This plot helps illustrate the change in the shape of the antenna radiation pattern as the maximum gain shifts from nadir to angles off nadir (i.e., resulting in a scalloped pattern) and back again. From Figure 16, it is noticed that the gain sensitivity to the ground plane offset is more than 18 dB—higher than that of the ground plane length and ground plane width parameter. Also, it can be concluded that for maximum gain, an antenna-ground plane offset of 0.15λ is required. The theory of images suggests that ideal antenna-ground plane spacing is 0.25λ, and this is the standard antenna-ground plane offset used in practice. This difference in the simulated result and image theory is that antenna image theory does not consider the loading effect of the ground plane on the antenna and simply considers the phase propagation of the forward-radiated and reflected fields. In addition, image theory assumes an infinite ground plane, which computationally results in an "image" of the antenna placed an equal distance on the other side of the ground plane to account for the reflection. In the case of a finite ground plane, the image concept is no longer applicable.

To extend the analysis, the ground plane offset range was extended up to two wavelengths. Figure 17 shows the nadir gain versus offset for the extended analysis, and it is noticed that when the offset distance is about 15%, 70%, 125%, or 175% of the wavelength, a local maximum gain at nadir is achieved. However, since the ground plane offset would represent the thickness of the airfoil (for antennas embedded in the lower wing skin) or the external offset of the antenna, it is ideal to keep h as small as possible in most cases. Hence, it is recommended that the antenna-ground plane offset be maintained to 15% of wavelength. A relationship for the minimum offset is given by

$$h_{\min} = 0.15\lambda. \tag{6}$$

In an effort to try to capture the antenna performance sensitivity to simultaneous changes in ground plane offset and width, a parametric analysis consisting of 220 simulations that systematically varied the ground plane offset from 0.05 to 1λ (with 0.05λ step size) and the ground plane

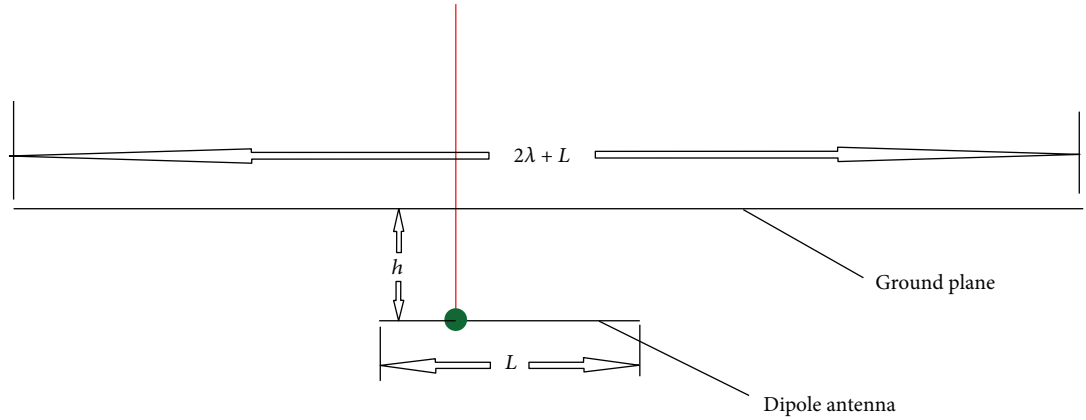

Figure 14: Ground plane offset defined for the wing offset study.

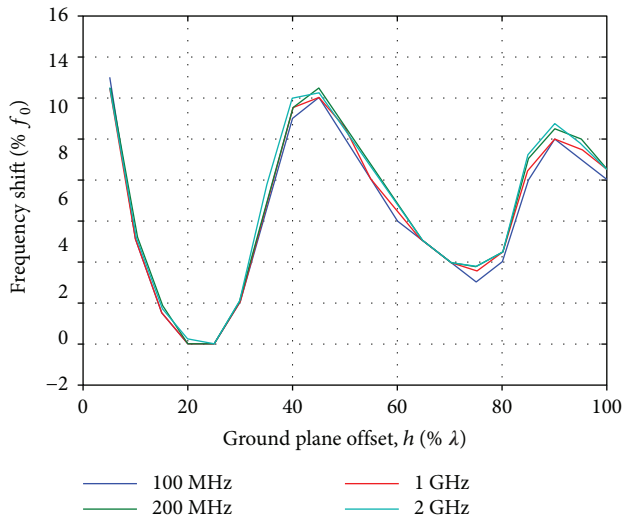

Figure 15: Frequency shift versus ground plane offset, h, in % λ.

width extension from 0.10 to 0.97λ (with 0.08λ step size) was performed at 100 MHz. The purpose of this analysis is to characterize the performance sensitivity when the ground plane offset is slightly off from the nominal spacing specified by 6. Figure 18 is a 3D plot with the nadir gain plotted against the ground plane width and antenna-ground plane offset. Both Figures 17 and 18 suggest that the ground plane-antenna offset should be kept within 10–20% or 65–75% of the wavelength for the gain to be within 1 dB of the local maximum gain. From Figure 18, it can be seen that this relationship holds true for all ground plane width extensions analyzed. From this observation, it could be concluded that an antenna array could be embedded in the lower wing skin and the upper skin could be used as a ground plane, so long as the wing chord length is between 0.6λ and 1.88λ. This range was found by assuming the ideal minimum antenna-ground plane offset (0.15λ) and typically t/c ratios of 8–25%.

3. Application of Sensor Study

The ground plane sizing simulations were repeated with a four-element antenna array to verify the trends obtained for the wing ground plane effects on a single antenna extend to multielement arrays where coupling is present. The array simulations included a modified dipole antenna that is identical to that which is flown on the NASA P-3 OIB installation shown in Figure 1. This modified dipole antenna is 0.74 m long and 0.14 m wide. Detailed information regarding this antenna design can be found in [31]. The array of four modified dipole antenna elements has an element spacing of 0.79 m, resulting in a 0.018 m gap between adjacent antennas as shown in Figure 19. A simulation setup similar to Section 2 was created for modified dipole antenna array using ANSYS HFSS [29] software.

3.1. Wing Span Trend Comparison. Initially, the spanwise length of the array ground plane was set to 4L (3.15 m) and subsequently extended on either side by varying the values of d (5–100% of the resonant wavelength with 5% increments). The chordwise width of the ground plane was kept constant at $W + 2\lambda$ (3.57 m), and a ground plane offset of $\lambda/4$ (0.43 m) was maintained. A parametric analysis was performed, and the normalized gain (normalized to its corresponding maximum gain) was plotted for both array and the single antenna results from Section 2.2 for comparison in Figure 20.

The gain response of the array is less sensitive to the ground plane length than the single element (<0.5 dB versus 1.5 dB). This is somewhat expected since only the end elements "see" the ground plane and are expected to be affected. While less obvious, the array gain also has an oscillatory response to the ground plane length. Though small, this variation is once again attributed to the cyclic response of the ground plane current.

Most interestingly about the array results is that the maximum gain still occurs at a ground plane extension of around 40%. The level of similarity between the individual element and array results was surprising since the ground plane design equations do not consider the cross-coupling between the elements. It was expected that the interelement coupling would dominate the response, and the applicability of the sizing relationships would be limited. Though the array response is much less sensitive to the ground plane extension than the single element, the maximum gain occurs at the

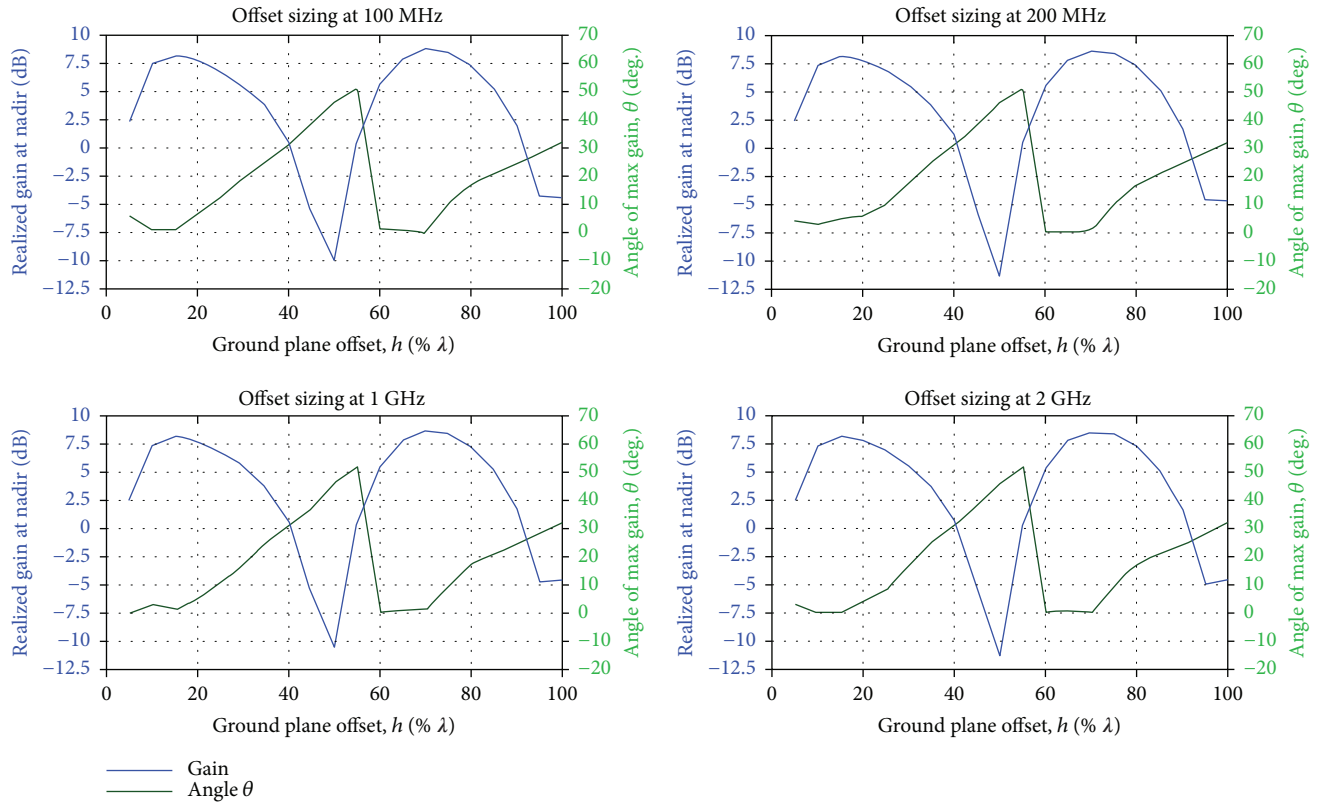

Figure 16: Ground plane offset versus realized gain at nadir and angle of max gain plot for all operating frequencies.

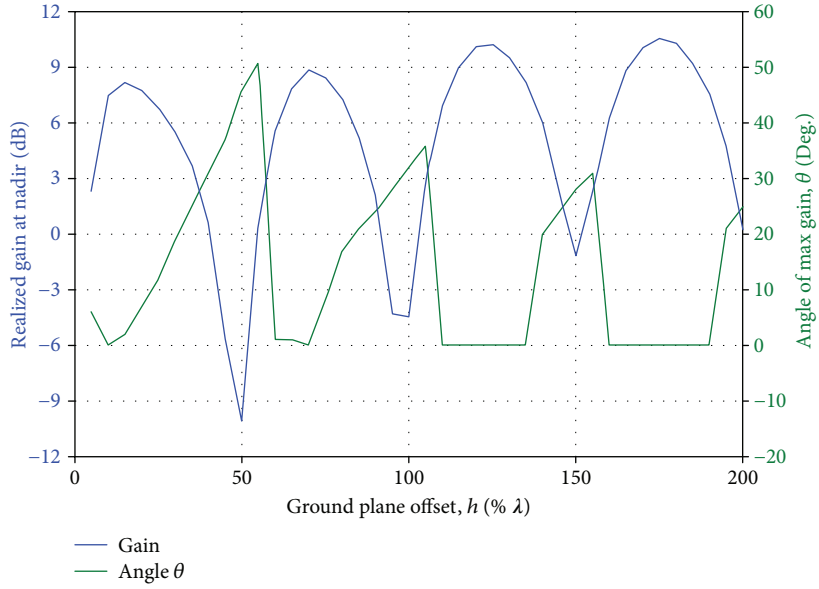

Figure 17: Ground plane offset up to 2 wavelengths versus realized gain at nadir and angle of maximum gain for all operating frequencies.

same extension value. The fact that the individual dipole element results and the dipole array results agree so well speaks to the robustness of the derived equations and greatly extends their use.

3.2. Wing Chord Trend Comparison. For the array chord study, the antenna-ground plane offset was set to be $\lambda/4$, and the length of the ground plane was set to be $4L + 2\lambda$ (6.58 m). Both parameters were kept constant while only the wing chord extension parameter was varied. Initially, the width of the ground plane was set equal to that of the antenna width ($W = 0.14$ m); then, the ground plane width extension parameter was varied from 5 to 100% of the resonating wavelength of 5% for the parametric analysis. The

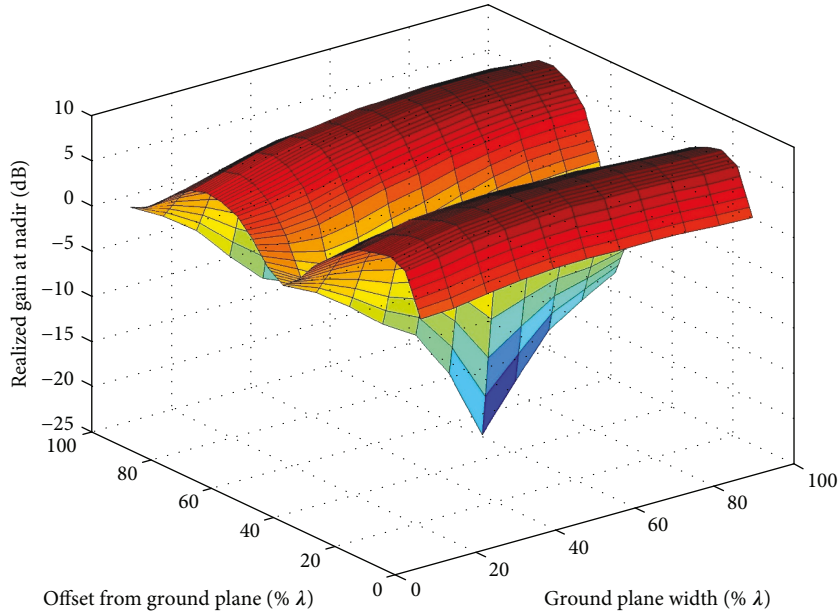

Figure 18: 3D plot showing gain relationship to ground plane width and offset.

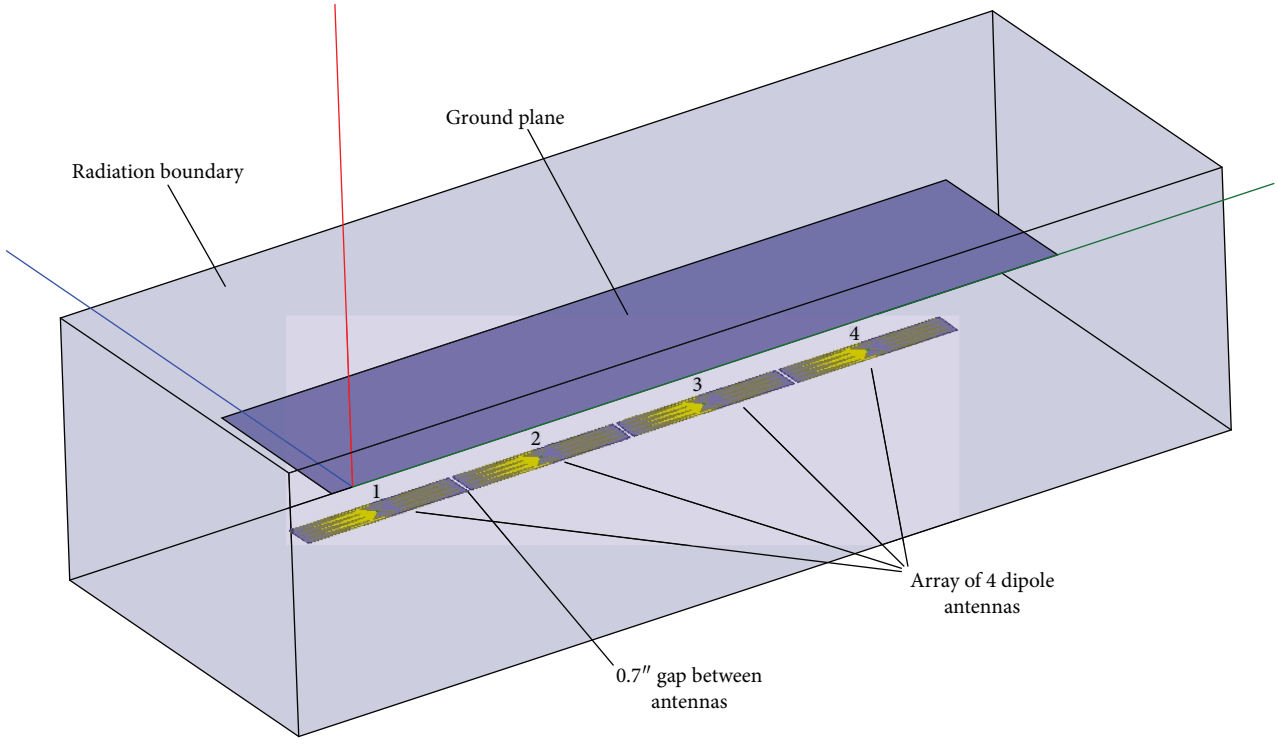

Figure 19: Four element dipole antenna array.

results for the normalized gain of the array are plotted against d in Figure 21 along with the results for the single element found in Section 2.3.

The array and single element have nearly identical response. More importantly, when d is ~50% of the wavelength, the maximum gain at nadir is achieved, supporting the relationship found for the wing ground plane chord in (4). The similarity between the single element and array (trends are within ~0.2 dB) is attributed to all elements in the array being affected by the variation in the width extension. Despite the existence of the coupling, the chord relationship developed for the single element appears to be robust and applicable for the array.

3.3. Wing Offset Trend Comparison. In this study, the ground plane length was set to $4L + 2\lambda$ (6.58 m) and the ground plane width was set to $W + 2\lambda$ (3.57 m). For this study, the offset distance h between the antenna array and the ground plane

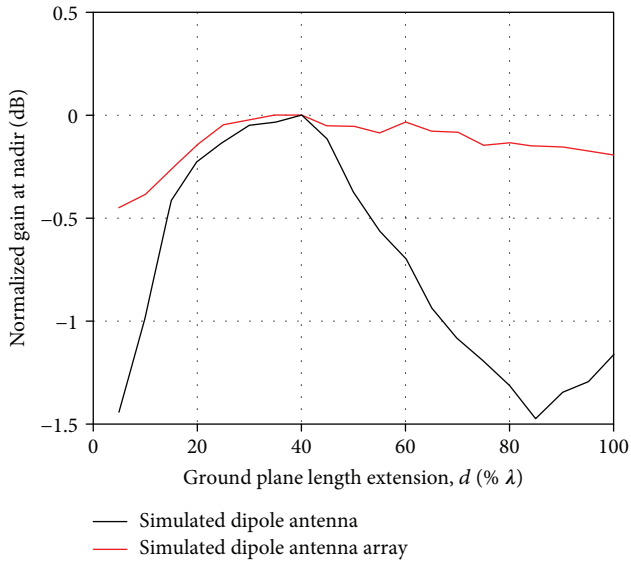

Figure 20: Comparing the ground plane length extension versus normalized gain at nadir for the single dipole element and array.

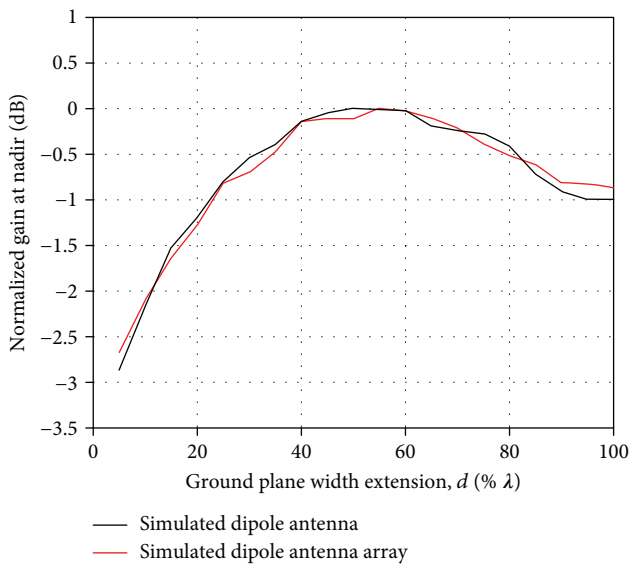

Figure 21: Comparing the ground plane width extension versus normalized gain at nadir for the single dipole element and array.

was varied from 5 to 40% of the resonating wavelength with increments of 5%. The normalized gain at nadir of the array is plotted against the ground plane offset parameter in Figure 22 along with a similar trend for the single dipole antenna from Section 2.4.

While there is some significant mismatch between the array and the single element for small offsets, the trends and the value for maximum gain are the same. Optimal antenna array performance is achieved when the antenna-ground plane offset is about 15% of its resonating wavelength. The variation seen in the trends is likely caused by the significant loading effects of the ground plane experienced by all elements. Despite the lack of coupling in the single element model, the gain response follows a similar trend,

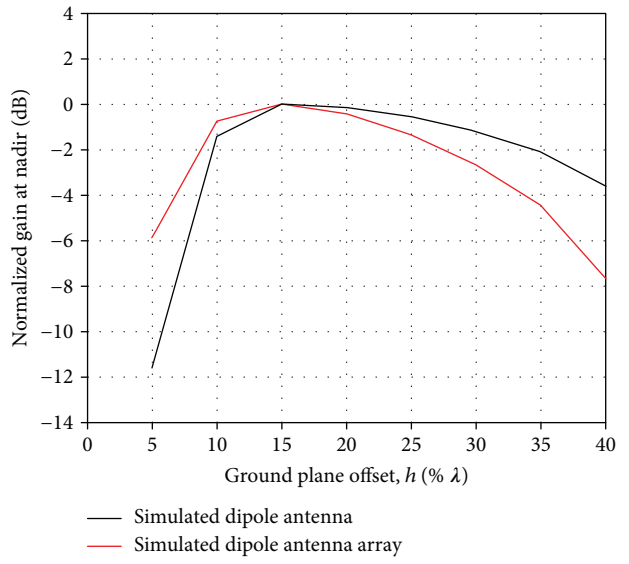

Figure 22: Comparing the ground plane offset versus normalized gain for the single dipole element and array.

namely, that the peak gain occurs for the same d value. The agreement of the optimal d value in both studies supports the offset relationship developed in Section 2.4.

At the end of this study, a parametric analysis of 160 simulations was performed to view the antenna array sensitivity to simultaneous changes ground plane offset and width. In this analysis, the ground plane width extension was set to 5–100% of resonant frequency wavelength and the ground plane offset was set to 5–40% of the resonating wavelength, with 5% increments each. The ground plane length was kept constant at $4L + 2\lambda$ (6.58 m). The trends obtained from the parametric analysis are plotted in Figure 23, where it can be noticed that the realized gain at nadir is much more sensitive to the ground plane offset than the width. When the width is varied in addition to the offset, the maximum gain still occurs when the offset is 0.15λ of a wavelength, and the absolute maximum gain occurs when the offset is 0.15λ and the width extension is 0.5λ, which confirms the relations found in Section 2.3 and Section 2.4 for the wing chord and wing height are applicable and reasonable.

4. Conclusion

The key role of a ground plane in antenna array performance inspired an investigation into a sensor-driven preliminary wing sizing methodology. Based on ideal antenna performance, relationships were derived for wing span, chord, and thickness (and thickness-to-chord ratio). In the context of the preliminary aircraft design methods of [27], it is expected that these relationships would be used after a wing-loading and power-loading design point has been selected; thus, the suggested span and chord derived from (2), (3), (4), and (5) would be constrained by the selected wing area. Various combinations of the span and chord relationships derived in this paper can be used to determine ranges of aspect ratios based on antenna performance. Similarly, the wing chord and thickness relationships can be used

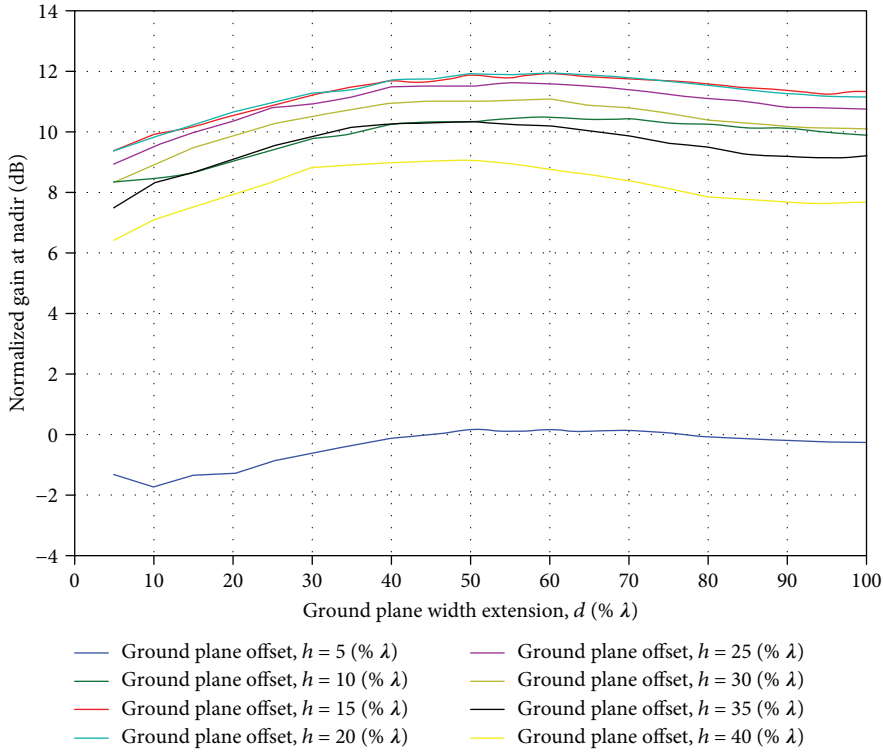

Figure 23: Comparing the ground plane width extension versus realized gain at nadir plots at different ground plane offsets.

to determine ideal airfoil t/c ranges and determine whether the antennas could be integrated internally or mounted externally to the wing.

It was found that the dipole antenna is the most sensitive to antenna-ground plane offset and least sensitive to the wing ground plane span, and only the antenna offset parameter resulted in any significant shift in the resonant frequency. This frequency sensitivity is due to the ground plane loading of the antenna changing as a function of the offset. For the maximum gains at 15% and 70%, the ground plane loading causes a downward shift in the ideal spacing (as compared to those suggested by image theory). With the larger offset maximums of 125% and 175% where the loading effects are negligible, the ideal spacing matches perfectly with the theory. Similar trends between the dipole antenna array and generic dipole antenna support the wing span, wing chord, and wing height relationships developed in Section 2. From this study, it can be concluded that the relationships developed for the single dipole antenna can be extended to entire dipole arrays, which greatly extends their use. However, these relationships should not be used for other antenna types without validation.

While this preliminary study shows promising results for utilizing empirical relationships for sizing future sensor structures, their use should still be limited because more detailed analysis is needed. For instance, the wing ground plane was idealized as a flat plate, but the curvature of an airfoil profile would be expected to affect the pointing of the radiation pattern. In addition, the antenna and antenna array simulations did not include any internal wing components (such as servos and cables), which can adversely interact with antennas. Wing flexure is also expected to affect the antenna array performance. Finally, the relationships derived are for the ground plane (conductive) portion of the wing; if the wing is not fully conductive, the relationships will need to be modified appropriately. Future studies will look at the effects of these aspects, and characterization of these sensitivities might allow for prediction of the as-installed antenna performance. Currently, the as-installed performance can only be predicted with full-wave 3D analysis or prototype measurements. This study serves as a foundation to refine these sizing relationships to consider more detailed design considerations.

Nomenclature

c: Wing chord
d: Ground plane extension parameter
EM: Electromagnetic
f: Operating frequency
F: Fuselage diameter
GP: Ground plane
H: Offset between wing and ground plane
L: Antenna length
λ: Wavelength
MAS: Multifunctional aircraft structures
UAS: Unmanned aircraft system
W: Antenna width.

Conflicts of Interest

The authors declare that they have no conflicts of interest.

Acknowledgments

This investigation was supported by the University of Kansas General Research Fund Allocation no. 2302032.

References

[1] F. Rodriguez-Morales, S. Gogineni, C. J. Leuschen et al., "Advanced multifrequency radar instrumentation for polar research," *IEEE Transactions on Geoscience and Remote Sensing*, vol. 52, no. 5, pp. 2824–2842, 2014.

[2] L. Li, G. Heymsfield, J. Carswell, D. Schaubert, J. Creticos, and M. Vega, "High-altitude imaging wind and rain airborne radar (HIWRAP)," in *IGARSS 2008 - 2008 IEEE International Geoscience and Remote Sensing Symposium*, pp. III - 354–III - 357, Boston, MA, USA, July 2008.

[3] R. F. Rincon, T. Fatoyinbo, K. J. Ranson et al., "Development of the EcoSAR P-band synthetic aperture radar," in *2012 IEEE International Geoscience and Remote Sensing Symposium*, pp. 4505–4508, Munich, Germany, July 2012.

[4] H. Schippers, J. H. van Tongeren, P. Knott, T. Deloues, P. Lacomme, and M. R. Scherbarth, "Vibrating antennas and compensation techniques NATO Task Group RTO/SET-087/RTG-50," in *2007 IEEE Aerospace Conference*, Big Sky, MT, USA, October 2008.

[5] C. Wang, B. Duan, F. Zhang, and M. Zhu, "Analysis of performance of active phased array antennas with distorted plane error," *International Journal of Electronics*, vol. 96, no. 5, pp. 549–559, 2009.

[6] E. J. Arnold, J.-B. Yan, R. D. Hale, F. Rodriguez-Morales, and P. Gogineni, "Identifying and compensating for phase center errors in wing-mounted phased arrays for ice sheet sounding," *IEEE Transactions on Antennas and Propagation*, vol. 62, no. 6, pp. 3416–3421, 2014.

[7] A. Ossowska, J. H. Kim, and W. Wiesbeck, "Influence of mechanical antenna distortions on the performance of the HRWS SAR system," in *2007 IEEE International Geoscience and Remote Sensing Symposium*, pp. 2152–2155, Barcelona, Spain, July 2007.

[8] P. Knott, "Deformation and vibration of conformal antenna arrays and compensation techniques," in *Paper presented at Multifunctional Structures/Integration of Sensors and Antennas, Paper 19*, Neuilly-sur-Seine, France, October 2006.

[9] E. J. Arnold, "Development and improvement of airborne remote sensing radar platforms," Ph.D. Dissertation, University of Kansas, Department of Aerospace Engineering, 2013.

[10] W. R. Donovan, "The design of an uninhabited air vehicle for remote sensing in the cryosphere," M.S. Thesis, Department of Aerospace Engineering, University of Kansas, Lawrence, Kansas, 2007.

[11] W. R. Donovan, R. D. Hale, and W. Liu, "Design and structural analysis of the meridian unmanned aircraft," in *49th AIAA/ASME/ASCE/AHS/ASC Structures, Structural Dynamics, and Materials Conference, 16th AIAA/ASME/AHS Adaptive Structures Conference,10th AIAA Non-Deterministic Approaches Conference*, Schaumburg, IL, USA, 2008.

[12] R. D. Hale, W. R. Donovan, and S. Keshmiri, *UAS Cryospheric Remote Sensing in the Center for Remote Sensing of Ice Sheets*, AUVSI's Unmanned Systems North America, Washington, DC, USA, 2009.

[13] W. R. Donovan, "The design of an uninhabited air vehicle for remote sensing in the cryosphere," M. S. Thesis, Aerospace Engineering Dept., University of Kansas, Lawrence, Kansas, 2007.

[14] B. Panzer, "Development of an electrically small Vivaldi antenna: the CReSIS aerial Vivaldi," MS Thesis, Department of Electrical Engineering, University of Kansas, Lawrence, Kansas, 2004.

[15] W. R. Donovan, D. M. Mueller, E. Runge, and W. Liu, "Structural design, analysis, and testing of Vivaldi ground penetrating radar antennas for the Meridian UAS," in *49th AIAA/ASME/ASCE/AHS/ASC Structures, Structural Dynamics, and Materials Conference, 16th AIAA/ASME/AHS Adaptive Structures Conference,10th AIAA Non-Deterministic Approaches Conference*, Schaumburg, IL, USA, 2008.

[16] Press, "Unmanned in Antarctica," sUAS News the business of drones, December 2015, http://www.suasnews.com/2014/01/unmanned-in-antarctica/, 28 January 2014.

[17] A. K. Bhattacharyya, "Effects of finite ground plane on the radiation characteristics of a circular patch antenna," *IEEE Transactions on Antennas and Propagation*, vol. 38, no. 2, pp. 152–159, 1990.

[18] A. M. Thomas, *Modern Antenna Design*, Wiley, Hoboken, NJ, USA, 2nd edition, 2005.

[19] S. Goswami, k. Sarmah, k.k. Sarma, and S. Baruah, "An approach for design of size independent simple microstrip antenna with complementary split ring resonator at ground plane," in *2015 International Conference on Signal Processing and Communication (ICSC)*, pp. 166–170, Noida, India, March 2015.

[20] J. Huang, "The finite ground plane effect on the microstrip antenna radiation patterns," *IEEE Transactions on Antennas and Propagation*, vol. 31, no. 4, pp. 649–653, 1983.

[21] E. Lier and K. Jakobsen, "Rectangular microstrip patch antennas with infinite and finite ground plane dimensions," *IEEE Transactions on Antennas and Propagation*, vol. 31, no. 6, pp. 978–984, 1983.

[22] S. Noghanian and L. Shafai, "Control of microstrip antenna radiation characteristics by ground plane size and shape," *IEE Proceedings - Microwaves, Antennas, and Propagation*, vol. 145, no. 3, pp. 207-208, 1998.

[23] M. T. Nguyen, B. Kim, H. Choo, and I. Park, "Effects of ground plane size on a square microstrip patch antenna designed on a low-permittivity substrate with an air gap," in *2010 International Workshop on Antenna Technology (iWAT)*, pp. 1–4, Lisbon, Portugal, March 2010.

[24] C. Peixeiro, "Small ground plane size effects on microstrip patch antennas revisited," in *2007 IEEE Antennas and Propagation Society International Symposium*, pp. 2821–2824, Honolulu, HI, USA, June 2007.

[25] G. Cung, G. H. Huff, and J. T. Bernhard, "Ground plane edge serrations for improved performance of microstrip active reflectarray elements," *IEEE Antennas and Wireless Propagation Letters*, vol. 2, no. 1, pp. 334–336, 2003.

[26] G. H. Huff and J. T. Bernhard, "Improvements in the performance of microstrip antennas on finite ground planes through ground plane edge serrations," *IEEE Microwave and Wireless Components Letters*, vol. 12, no. 8, pp. 308–310, 2002.

[27] J. Roskam, *Airplane Design I-VII*, DARcorporation, Lawrence, Kansas, 2nd edition, 2003.

[28] D. P. Raymer, *Aircraft Design: A Conceptual Approach*, AIAA Education Series, AIAA, New York, USA, 5th edition, 2012.

[29] HFSS, *High Frequency Structure Simulator*, Software Package, Ansys, Ver. 15.0.7, Canonsburg, PA, USA, 2014.

[30] C. A. Balanis, *Antenna Theory, Analysis and Design*, Wiley, Hoboken, NJ, USA, 3rd edition, 2005.

[31] K. J. Byers, A. R. Harish, S. A. Seguin et al., "A modified wide-band dipole antenna for an airobrne VHF ice-penetrating radar," *IEEE Transactions on Instrumentation and Measurement*, vol. 61, no. 5, pp. 1435–1444, 2012.